INFLUENCE OF MICROSTRUCTURE ON THE FRACTURE TOUGHNESS OF TEMPERED MARTENSITIC ALLOY STEELS

S. Slatcher[1] and J.F. Knott[2]

Air-melted and electroslag-refined versions of a NiCrMoV steel and air-melted and vacuum-arc-remelted versions of a NiCrMo steel have been studied. Different tempering temperatures in the range 150-680°C were used to produce a range of microstructures. It appears that the initiation of voids at carbides is the important event which determines the fracture toughness of these steels. The fracture toughness is related to a critical strain, and the variation of this critical strain with tempering temperature is discussed in terms of work hardening rate.

INTRODUCTION

Although much progress has been made in the understanding of the influence of microstructure on fracture toughness, the microstructure of engineering alloys is usually complex and it is not always possible to use simplistic models to describe such systems. For the case of quenched and tempered steels, it would usually be assumed that, when the fracture mode is fibrous, higher fracture toughnesses would be achieved by selecting materials which were "clean" in terms of inclusion content, and which possessed a high work hardening rate. Evidence from the study reported in this paper shows that these assumptions are not necessarily correct.

MATERIALS

The materials studied were:

(i) An air-melted version of a NiCrMoV steel (DAO or DAI)
(ii) An electroslag-refined version of a NiCrMoV steel (DEO or DEI)
(iii) An air-melted version of a NiCrMo steel (En25A)
(iv) A vacuum-arc-remelted version of a NiCrMo steel (En25V)

The NiCrMoV steel was supplied as 305mm diameter cylindrical forgings, and samples of this steel have the designation DAO or DEO if they were taken from the outer region of these forgings (at a radius of approximately 125mm), and the designation DAI or DEI of they were taken from the inner region (at a radius of approximately 65mm). The NiCrMo steel was supplied as 29mm diameter bar, which was forged down to give a 25mm square bar prior to any examination or testing of the material.

1 Det norske Veritas, P.O. Box 300, N-1322 Høvik, Norway

2 Dept. Metallurgy & Mat. Sci., University of Cambridge, Pembroke Street, Cambridge CB2 3QZ, U.K.

TABLE 1 - Chemical Analysis

	Weight %									
	C	Mn	S	P	Si	O	Ni	Cr	Mo	V
DAO	0.33	0.56	0.006	0.012	0.20	0.0040	3.2	1.15	0.69	0.22
DAI	0.30	0.55	0.006	0.010	0.19	0.0055	3.1	1.13	0.68	0.20
DEO	0.36	0.44	0.004	0.010	0.18	0.0045	3.1	0.79	0.69	0.22
DEI	0.36	0.45	0.003	0.011	0.15	—	3.2	0.78	0.70	0.22
En25A	0.34	0.72	0.012	0.012	0.19	0.0040	2.72	0.62	0.55	—
En25V	0.34	0.60	0.009	0.008	0.32	0.0025	2.76	0.75	0.59	—

From an EDS analysis of the non-metallic inclusions, it was inferred that the two predominant inclusion types in each steel were manganese sulphides, of chemical composition MnS, and oxides with a chemical composition close to $3MnO.\ Al_2O_3.\ 3SiO_2$. Knowing the chemical composition and the density of each inclusion type present, inclusion volume fractions, V_V, were calculated from the bulk oxygen and sulphur analyses of the steels (ref. 1).

TABLE 2 - Non-Metallic Inclusion Parameters

	DAO	DAI	DEO	DEI	En25A	En25V
$V_V/10^{-6}$	400	490	330	∿150	790	500
$\overline{\lambda}_V/\mu m$	19	18	18	20	14	17

The value of V_V for DEI is an estimate based on image analysing computer measurements, as the oxygen analysis is not available for this steel. It may be seen that the electroslag-refined and the vacuum-arc-remelted versions of the steels both contained substantially lower volume fractions of inclusions than their corresponding air-melted versions, and that the NiCrMo steel was generally "dirtier" than the NiCrMoV steel. Also tabulated above are the estimated mean nearest neighbour distances of inclusions having a maximum feret diamter on a random 2D section of greater than 1.44μm. It is difficult however to interpret the inclusion spacing results because, due to the sizing criterion, an inclusion refining effect could either increase or decrease the measured inclusion spacing.

The NiCrMoV steels were given an austenitising treatment of 3 hours at 910°C, oil quenched, and tempered for 2 hours at a temperature in the range 300-680°C followed by a water quench. The NiCrMo steel was given an austenitising treatment of 4 hours at 950°C, oil quenched, and tempered for 2 hours at a temperature in the range 150-600°C.

Figs. 1 and 2 show transmission electron micrographs of DAO tempered at 600 and 680°C respectively. The coarse elongated carbides in the microstructure of the 600°C temper were also present in the 350°C temper. There is also some carbide spheroidisation at 600°C, and in the 680°C temper the spheroidisation process is much more advanced. The martensitic plate structure, which remained intact at tempering temperatures upto 600°C, degenerated during the 680°C temper, resulting in a more polygonal grain structure, the grain boundaries often being pinned by large carbides. In addition to the coarse

carbides readily visible in fig. 1., a fine distribution of alloy carbides would be expected to be present in the steel tempered at 600°C (ref. 2). These fine alloy carbides would redissolve at 680°C.

Cylindrical tensile testpieces (Hounsfield No.I3)were machined such that the loading axes were parallel to the maximum stresses in the fracture toughness testpieces. In fig. 3, the 0.2% proof stress, σy, is plotted against tempering temperature for each steel.

FRACTURE TOUGHNESS

The design and loading modes of the fracture toughness testpieces were as follows:

NiCrMoV steel: breadth = width = 25mm,
crack length ∿12½mm, 4 point bend, span = 100mm, bending arm = 25mm.
NiCrMo steel: breadth = width = 20mm,
crack length ∿10mm, 3 point bend, span = 80mm.

The NiCrMoV steel testpieces were taken in the Y-Z orientation and the NiCrMo steel testpieces in the X-Y orientation, as defined in ref. 3 . All NiCrMoV steels tempered at temeratures under 500°C gave "valid" K_{IC} values which were converted to initiation crack opening displacement, δ_i , values using the relation

$$\delta_i = \frac{K_{IC}^2(1-\nu^2)}{\sigma_y E}$$

and these values are shown plotted in fig. 4. The 150°C temper of the NiCrMo steel also gave "valid" K_{IC} values, but the δ_i values plotted in fig. 4 were obtained from stretch zone measurements (ref. 4). Other δ_i values were obtained by extrapolating R-curves to zero fibrous crack extension. Measurements made on silicone rubber crack tip replicas revealed that crack opening displacement values calculated according to BS 5762(ref. 5) underestimate the true values for these steels by approximately 40%. Therefore curves similar to those in (ref. 6) were used to convert calculated values of δ_i to the "replica" values of δ_i which are plotted in fig. 4.

It is apparent that the inclusion content of these steels does not have a marked effect on their toughnesses, and also that, by varying the tempering temperature, order of magnitude changes in δ_i may be obtained. Therefore it may be deduced that it is the tempered martensitic microstructure which plays the most important role in determining the fracture toughness of such steels. Also, it may be noted that varying the tempering temperature has a much larger effect on the toughness than it does on the 0.2% proof stress. This suggests that the large toughness variations are not merely the result of varying the strengthof the steels, but that they have a more direct link with the microstructural changes accompanying them.

CRITICAL FRACTURE STRAIN

The cracks in these steels were all ductile and generally had a zig-zag profile (see fig. 5). The fact that the fracture surface profiles of each side of the crack seem to fit together reasonably well indicates that the fracture process zone is confined to a relatively narrow region along the surfaces of the resultant crack. This was confirmed by more detailed metallography in a region just ahead of the crack-tip; fig. 6 shows a fine

non-crystallographic crack which may have been formed by the coalescence of voids initiated at carbides. Also, in support of this hypothesis, the fracture surfaces show evidence of ductile dimples (fig. 7), the spacing of which seems to correspond approximately to that of the larger carbides.

If, then, it is assumed that it is the coalescence of voids formed around carbides which is the important micromechanism of fracture, then it is likely that fracture would occur at a critical strain, ε_C, and that the initiation of fracture from an originally sharp crack would occur at the crack opening displacement which corresponds to ε_C being attained over a critical distance. It seems likely that the ductile crack extends in a step-wise fashion, each step corresponding to a straight region in its zig-zag path. It is therefore reasonable to take the step length to be the distance over which the critical strain must be attained. In fig. 5 it may be seen that the average step length is approximately 70 μm, which corresponds to about $4\bar{\lambda}_v$. Taking, therefore, the critical distance to be $4\bar{\lambda}_v$ for each steel and using Willoughby's experimentally determined strain distribution (ref. 7), critical strains may be calculated. The critical strains for the NiCrMoV steel are shown plotted in fig. 10. Fracture strains were also measured for a few NiCrMoV steels using plane strain tensile testpieces of a design similar to that of Clausing's (ref. 8) with the loading axes parallel to the maximum stresses in the fracture toughness testpieces, and these results are also plotted on fig. 8. It is an interesting finding that all the measured fracture strains fall within the scatter band of critical strains. It should be noted that fracture strains measured on cylindrical tensile testpieces are approximately 0.6 for the NiCrMoV steel and to not show nearly so much percentage variation with tempering temperature as do the plane strain fracture strains.

WORK HARDENING RATE

On examination of metallographic sections of propagating cracks, very little evidence was found of voids, around carbides or non-metallic inclusions, which had not coalesced. It may therefore be concluded that immediately following void initiation, the voids rapidly grow and coalesce under the influence of the high hydrostatic stresses found ahead of the crack tip. The critical strain ε_C could therefore be regarded as an initiation strain for voids formed at carbides. As Brown and Stobbs (ref. 9) pointed out, the carbide/matrix interface probably decoheres at a critical interfacial stress, σ_C, but the stress is the result of dislocation pile-ups at the carbides, therefore decohesion may be said to occur at a critical strain. This critical strain may be expected to vary with tempering temperature for several reasons:

(i) Some of the variation of ε_C is probably explicable in terms of changes in the carbide/matrix interfacial strength. The composition of the carbides may be expected to vary with tempering temperature in the range 550-650°C, and these compositional changes may lead to significant variations in σ_C. Also, the diffusion of impurities to the carbide/matrix interfaces during tempering may have a large effect on σ_C (ref. 10).

(ii) Brown and Stobbs (ref.9) predict that the initiation strain should be proportional to the particle radius. This suggests larger values of ε_C for higher tempering temperatures.

(iii) The effects of changing carbide shape with tempering temperature may also be large, not only because decohesion may be facilitated, but also, perhaps, because platelike carbides may crack to produce noid nuclei at low plastic strains.

(iv) In the case of martensitic steels, it is important also to consider the effect of tempering temperature on the dislocation density. Steels tempered at lower temperatures contain carbides with considerable dislocation tangles around them prior to any deformation, so it might be expected that these would have lower fracture strains than steels with an identical particle distribution but few dislocation.

Bearing in mind that the frature micromechanisms in these steels are likely to depend very much on the interaction of dislocations and carbides, i.e. local work hardening behaviour, one might expect that the fracture strains, and hence fracture toughness values, would be related to the macroscopic work hardening characteristics of the steels. Fig. 11 shows how the work hardening rate R varies with tempering temperature. R is the average work hardening rate between a plastic strain of 0.2% and the instability strain. Notice that generally (in the tempering temperature range 150-600^{o}C) there is a trend for lower work hardening rates to be associated with higher toughnesses. This is contrary to what might be expected considering the experimental evidence of other alloy systems (the aluminium alloys, for example of ref. 11), and most theoretical predictions (ref. 12 for example). However, it must be remembered that the high initial work hardening rates in steels are generally achieved by the interaction of dislocations and large carbides which leads to high carbide/matrix interfacial stresses and void initiation. The presence of large strengthening particle in aluminium alloys also leads to low toughnesses, but low work hardening rates result because the particles are readily cut. It is therfore clearly necessary to consider both work hardening and fracture micromechanisms before realistic links between work hardeningrates and fracture toughnesses may be obtained.

CONCLUSIONS

(i) The inclusion volume fraction has little effect on the fracture toughness of these tempered martensitic alloy steels.

(ii) For a range of tempering temperatures, the strain at a critical distance ahead of the crack tip at fracture initiation corresponds to the plane strain fracture strain, as measured using tensile testpieces.

(iii) Generally, the fracture toughness of these steels is inversely correlated with the work hardening rate. This is probably because the same micromechanism which leads to high work hardening rates in these steels also leads to the initiation of voids at carbides and therefore lower fracture strains.

ACKNOWLEDGEMENTS

The authors wish to thank the Ministry of Defence, Procurement Executive, for providing the financial support for this work, and Professor R.W.K. Honeycombe for making available the necessary research facilities. The assistance of Dr. H.K.D.H. Bhadesia and Dr. C.A. Hippsley is also gratefully acknowledged.

SYMBOLS USED

V_v - inclusion volume fraction

$\overline{\lambda}_v$ - mean nearest neighbour inclusion spacing

σ_y - 0.2% proof stress

δ_i - initiation crack opening displacement

K_{IC} fracture toughness

ν - Poisson's ratio

E - Young's modulus

ε_c - critical strain

ε_f - fracture strain measured on plane strain tensile testpieces

R - work hardening rate

REFERENCES

1. Franklin,A.G.,1969, Journal of The Iron and Steel Institute, volume 207,181-186.

2. Speich,G.R. and Leslie,W.C.,1972, Metallurgical Transactions, volume 3,1043-1054.

3. British Standards Institution,1977, Methods of test for plane strain fracture toughness(K_{IC})of metallic materials,BS 5447:1977.

4. Slatcher,S. and Knott,J.F.,1980, Advances in Fracture Research, Ed. Francois, Pergamon Press, 201-207.

5. British Standards Institution,1979, Methods for crack opening displacement(COD)testing, BS 5762:1979.

6. Slatcher,S. and Knott,J.F.,1981, International Journal of Fracture, volume 17,R109-114.

7. Willoughby,A.A.,Pratt,P.L., and Baker, T.J.,1980, Advances in Fracture Research, Ed. Francois, Pergamon Press, 179-186.

8. Clausing,D.P.,1970, International Journal of Fracture, volume 6, 71-84.

9. Brown,L.M., and Stobbs,W.M.,1976, Philosophical Magazine, volume 34, 351.

10. King,J.E., and Knott,J.F.,1981, Metal Science, volume 15, 1-6.

11. Chen,C.Q., and Knott,J.F., 1981, Metal Science, volume 15, 357-364.

12. Hahn,G.T., and Rosenfield,A.R., 1968, Applications Related Phenomena in Titanium Alloys, ASTM STP 432, 5-32.

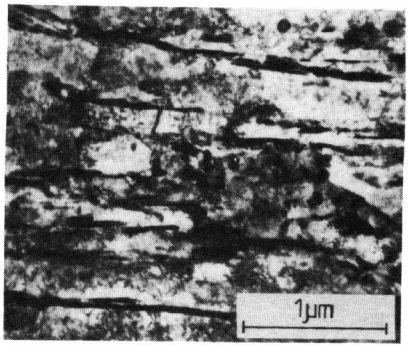

Fig. 1 The microstructure of DAO tempered at 600°C (courtesy Dr. H.K.D.H. Bhadesia).

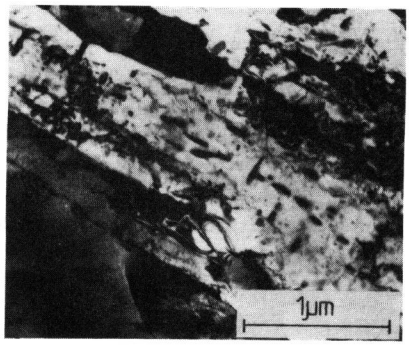

Fig. 2 The microstructure of DAO tempered at 680°C (courtesy Dr. H.K.D.H. Bhadesia).

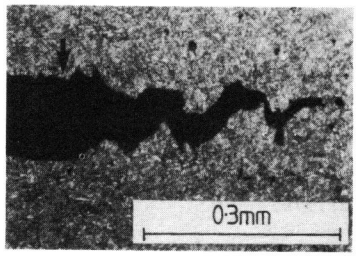

Fig. 5 The zig-zag fracture path of the ductile crack in the En25V tempered at 600°C. The position of the fatigue precrack tip is arrowed.

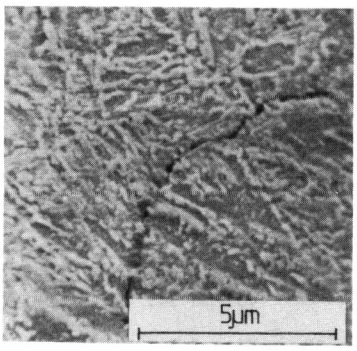

Fig. 6 A fine crack, just ahead of the main crack in the En25A tempered at 600°C.

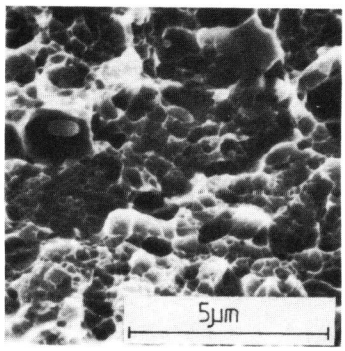

Fig. 7 Ductile dimples on the fracture surface of steel DEO tempered at 350°C.

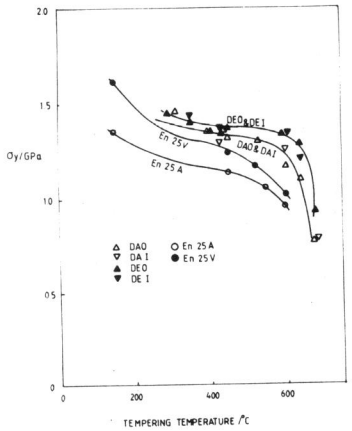

Fig. 3 The variation of 0.2% proof stress with tempering temperature.

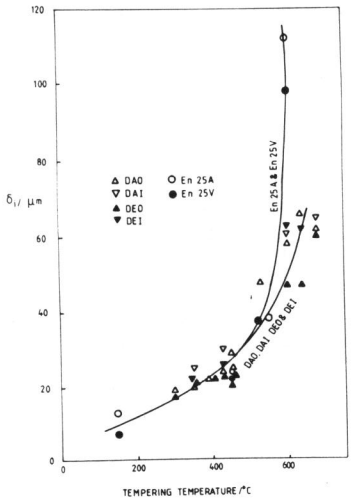

Fig. 4 The variation of initiation crack opening displacement with tempering temperature.

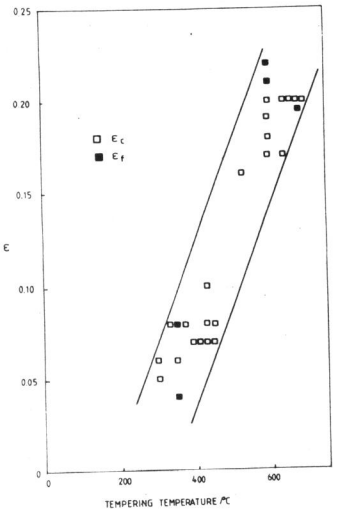

Fig. 8 The variation with tempering temperature of the critical strain, ε_c, ahead of the crack tip and the fracture strain, ε_f, measured on plane strain tensile testpieces.

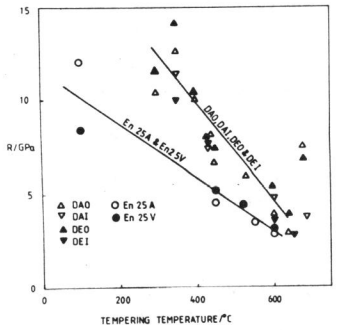

Fig. 9 The variation of work hardening rate with tempering temperature.